SYNTHESIS OF Fe_3O_4-BASED CATALYSTS FOR THE HIGH TEMPERATURE WATER GAS SHIFT REACTION

C. Martos; J. Dufour*; A. Ruiz

Department of Chemical and Environmental Technology, ESCET, Universidad Rey Juan Carlos

C/ Tulipán s/n, 28933 Móstoles, Madrid, Spain

Published on:

International Journal of Hydrogen Energy 34 (2009) 4475-4481

doi:10.1016/j.ijhydene.2008.08.042

Abstract:

The water gas shift reaction is an essential process to adjust the CO/H_2 ratio in the industrial production of hydrogen. FeCr catalysts have been widely used in this reaction at high temperature but have environmental and safety concerns related to chromium content. In this work the replacement of chromium by molybdenum in magnetite-based catalysts is studied. The materials were prepared by oxidation-precipitation and wet impregnation and they were characterized using X-ray powder diffraction, X-ray fluorescence, transmission electron microscopy and temperature programmed reduction. Specific surface areas of samples were also measured. The results obtained indicate that molybdenum increases thermal stability of the magnetite active phase and prevents metallic iron formation during the reaction. The oxidation-precipitation method allows obtaining the material directly in the active phase and molybdenum is incorporated into magnetite lattice.

Keywords: WGS, Cr-free catalysts, oxidation-precipitation.

* Corresponding author: tel.: +34914888138; fax: +34914887068.

E-mail address: javier.dufour@urjc.es

1. Introduction.

Nowadays, hydrogen is mostly being produced from fossil fuels like natural gas, liquid hydrocarbons and coal. In these processes, carbon is converted to CO_2 and released to atmosphere, leading to global climate change. Biomass is one of the most promising and sustainable resources to produce hydrogen because it can be considered as a CO_2 neutral precursor. Biomass materials can be converted to energy via thermochemical and biological processes [1]. There are two main thermochemical processes to produce hydrogen from biomass: (1) gasification, and (2) fast pyrolysis followed by reforming of the bio-oil produced [2-3]. Hydrogen can be also produced by steam reforming of the biomass derived oxygenates. In this context, steam reforming of ethanol is very attractive because this compound can be produced by fermentation from several biomass sources, is easy to store and is non-toxic [4-7]. However, all these processes produce carbon monoxide in association with hydrogen and CO concentrations over 10-50 ppm leads to deactivation of electrodes in fuel cell. The water gas shift reaction ($CO + H_2O \leftrightarrow CO_2 + H_2$) is essential to increase hydrogen production and to decrease the CO concentration to the desired value for these applications [8-9].

The water gas shift (WGS) reaction is reversible and moderately exothermic, being thermodynamically limited at high temperatures. Nevertheless, high temperatures are required to increase the reaction rate. Therefore, the WGS reaction is usually carried out in two stages. The first step at a temperature between 310 and 450 ºC using a catalyst based on Fe_3O_4-Cr_2O_3-CuO, which reduces CO concentration to 3 mol%. In the second stage, a catalyst based on Cu-ZnO-Al_2O_3 that operates at 210-240 ºC is used and the CO content is reduced to 0,3 mol% [10].

The high temperature WGS catalysts contain iron oxide structurally promoted with chromium oxide (8-14 wt%). The active phase of the catalyst is magnetite (Fe_3O_4), which in the absence of chromium oxide rapidly loses activity due to reduction in surface area by sintering. The role of chromia is mainly to stabilise the material, although recent studies have shown that it can also catalyse the reaction, but in a lower extension than iron oxide. Furthermore, the commercially available catalysts contain a small amount of copper as an activity and selectivity enhancer. These catalysts are often synthesized by a coprecipitation method as Fe_2O_3, and reduced to the active phase. The reduction process is highly exothermic and should be controlled to avoid the production of metallic iron, which may catalyze undesirable reactions. In industrial processes, large amounts of steam are used to inhibit metallic iron formation, but this implies high operational costs [11]. An interesting alternative to prepare these materials directly in the active phase is the oxidation-precipitation method [12].

The catalysts based on Fe_3O_4-Cr_2O_3 have environmental and safety problems related to chromium compounds [13]. Furthermore, exposure to liquid water originated from condensation in catalytic reactors should be avoided, because of possible chromate leaching [14]. Therefore, the search for non-toxic catalysts that could be easily handled and discarded is much needed. There are several studies to replace chromium by other promoters like V, Al, Mo, Th and Mn [15-18]. Li and co-workers studied the replacement of Cr by Mo in coprecipitated catalysts. These materials were as active as the commercial one [17]. However, the replacement of chromium by other element could lead to the sintering of the catalysts at reaction temperatures and it is necessary to modify them to improve their performance.

The objective of this work is to study the replacement of Cr by molybdenum keeping the activity of catalysts based on Fe_3O_4. Oxidation-precipitation and wet impregnation methods were studied to prepare these materials.

2. Experimental.

2.1. Catalysts preparation

Two series of samples were synthesized for this study and were denoted A and B. Catalysts A were prepared by oxidation-precipitation of an aqueous solution of metal salts using NH_4OH or NaOH as precipitating agent. Four types of samples were prepared: (i) with iron and chromium (AFeCr); (ii) with iron, chromium and copper (AFeCrCu); (iii) with iron and molybdenum with different Fe/Mo ratios (AFeMo12, AFeMo20 and AFeMo53); and (iv) with iron, molybdenum and copper (AFeMoCu).Table 1 shows the theoretical Fe/promoter ratios used to prepare these materials.

Initially, an aqueous solution of $FeCl_2$, $CuCl_2$, $CrCl_3$ or $(NH_4)_6Mo_7O_{24}$ were prepared with appropriate Fe/promoter molar ratios and were heated up to 70 ºC. Next, the solution was stirred at 300 r.p.m. and was oxidized bubbling air into the system. Alkali was added drop-wise adjusting pH of the system to 7 until the end of reaction. The solid was recovered by filtration and washed out with water to remove ions. Finally, the samples were dried at 70ºC overnight.

Catalyst B was prepared by wet impregnation of Fe_3O_4 synthesized by oxidation-precipitation, with an aqueous solution of $(NH_4)_6Mo_7O_{24}$. These materials were dried at 70 ºC overnight and calcined at 500 for 3 h. The theoretical Fe/Mo ratio of sample BFeMo is shown in Table 1.

2.1. Catalysts characterization

X-ray powder diffraction (XRD) patterns of the catalysts were obtained on a Philips X-

Pert diffractometer using Cu Kα radiation. The data were recorded in the 2θ range from 10º to 70º. Average crystallite sizes were calculated by applying the Scherrer equation. X-ray fluorescence (XRF) spectrometer Philips MagiX was used to determine Fe/promoter ratio. Transmission electron microscopy (TEM) micrographs were obtained on a Philips Tecnai-20 electron microscope operating at 200 kV and equipped with an energy dispersive X-ray (EDX) spectrometer. Temperature programmed reduction (TPR) was performed in a Micromeritics Autochem 2910 instrument. The sample (50 mg) was heated up from 323 K to 1173 K (heating rate 10 K/min) under a hydrogen-argon mixture (10 % H_2) with a flow rate of 40 ml/min. Specific surface areas of samples were calculated from N_2 adsorption-desorption isotherms at 77 K, that were measured on a Micromeritics TRISTAR 2050 instrument.

2.3. Catalytic Activity test

The performance of catalysts was tested in a fixed bed stainless steel reactor (i. d. = 9 mm) under isothermal conditions (380 ºC), 10 bar and GHSV = 10000 h^{-1}. All experiments were carried out using 4,5 g of catalyst (250-355 µm). The composition of fed gas corresponded to a theoretical biomass gasification gas: 40 % H_2, 44 % CO and 16 % CO_2. A low steam/CO ratio was added to the reactor to simulate the membrane reactor conditions. Therefore, a H_2O/CO molar ratio of 2 was employed. The product stream was analyzed by gas chromatography in a Varian CP-4900 Micro GC.

3. Results and discussion

3.1. Synthesis of high temperature WGS catalysts by oxidation-precipitation

Oxidation-precipitation method was employed to prepare Fe_3O_4-Cr_2O_3-CuO catalyst directly in the active phase. The material obtained was compared with a commercial one to study the feasibility of oxidation-precipitation as synthesis method for conventional high temperature WGS catalyst. Figure 1 shows XRD patterns of AFeCrCu material. Magnetite

was the only crystalline phase detected in this sample and separate chromium or copper phases were not observed by this technique. Copper phases did not appear in the diffractogram because of the lower content of this metal in the material. In the other hand, chromium could form a mixed oxide with iron ($FeCr_2O_4$) and the diffraction lines of this compound are in coincidence with those of magnetite. TPR results are shown in Figure 2. There were two main reduction peaks. The lower temperature peak was attributed to reduction of Fe^{3+} species to Fe_3O_4, Cu^{2+} to metallic copper and Cr^{6+} to Cr^{3+}. The last broad peak was due to reduction of Fe_3O_4 to FeO and metallic iron. FeCrCu catalysts prepared by oxidation precipitation showed a TPR profile similar to that of the commercial one. The second reduction peak for FeCrCu catalyst was observed at 605 º C, whereas for commercial material this reduction occurred at 716 ºC. This increase of reducibility for sample prepared by oxidation-precipitation could indicate that the particle size of this material was lower. The BET surface area of the material prepared by oxidation-precipitation (109 m^2/g) was higher than the commercial one (69 m^2/g), confirming its lower particle size.

Samples were tested under WGS reaction conditions, obtaining a similar CO conversion for both catalysts in the same reaction time. Product distribution obtained under reaction is shown in Table 2. CO concentration decreased below 10 %Vol. for both samples studied. Hydrogen concentration in the product gas was over 55 %Vol. These results indicated that oxidation-precipitation method allows obtaining high temperature WGS catalysts directly in the active phase and the behaviour of them were similar to the commercial one under the reaction conditions studied.

3.2. Replacement of chromium by molybdenum

The X-ray diffractograms of AFeCr, AFeMo12 and BFeMo samples are shown in Figure 3. Magnetite was the only crystalline phase in the molybdenum sample synthesized by oxidation-precipitation (AFeMo12). Figure 4 shows the electron diffraction pattern obtained

from catalyst prepared by wet impregnation and indicates that it consisted of γ-Fe_2O_3. This result was expected because this material was calcined up to 500 ºC to incorporate molybdenum into the magnetite lattice. So, it was not obtained in the active phase. Therefore, catalysts obtained by impregnation (BFeMo) must be reduced to Fe_3O_4 to be active in WGS reaction.

Comparing the samples prepared with chromium (AFeCr) and molybdenum (AFeMo12) by oxidation-precipitation, Figure 3 shows their XRD patterns. Magnetite was the crystalline phase detected in both samples and chromium or molybdenum segregated phases were not observed. Lattice parameters (ao) were calculated from higher intensity lines of XRD patterns for each sample and are shown in Table 3. The presence of Mo in the catalyst produced a decrease of the magnetite phase lattice parameter from 0,8399 to 0,8353 nm. Mo^{6+} possess an ionic radius (0,73 Å) smaller than Fe^{3+} (0,785 Å) and Fe^{2+} (0,74 Å) , leading to a reduction in cell parameter. In the case of AFeCr sample the contraction of the lattice parameter was lower since Cr^{3+} ionic radius (0,755 Å) is larger than that for Mo^{6+}. Average crystallite sizes (Dc) were calculated from XRD patterns by Scherrer equation. The crystallite size of AFeCr catalyst was lower than that obtained for AFeMo12. It has been reported that substitution of iron by larger metal ions generates stress in the system. The equilibrium particle size is then shifted towards smaller particles to overcome this stress, because the ratio of strain to surface effects becomes greater for larger particles [19]. Therefore, the lower crystallite size of AFeCr sample could be explained by the larger ionic radius of Cr^{3+}.

TEM microphotographs of AFeCr and AFeMo12 samples are shown in Figure 6. Both materials were composed of spherical crystals with sizes in the range of 20-100 nm and the particle morphology was homogeneous. The results obtained by energy dispersive X-ray (EDX) indicated that AFeCr material was composed of Fe_3O_4 crystals (Fe/Cr = 110) surrounded by smaller high chromium containing particles (Fe/Cr = 4,6). However, in the case of molybdenum catalysts the promoter was incorporated into the magnetite lattice and

EDX analysis showed that there was not a considerable variation in the molybdenum content in different crystals.

Table 3 shows XRF results and specific surface areas for these samples. There was no variation in the molybdenum content for both synthesis methods, but BET surface area was higher for sample obtained by oxidation-precipitation (AFeMo12), since it was not calcined. Specific surface area obtained for AFeCr catalyst was 106 m^2/g whereas for molybdenum material (AFeMo12) was 32 m^2/g. The higher BET surface area obtained for chromium catalyst could be related with the presence of smaller high chromium containing particles surrounding magnetite crystals. However, molybdenum was incorporated into magnetite lattice for AFeMo12 sample, obtaining a lower BET surface area in this case.

To study changes in catalysts reducibility, molybdenum and chromium catalysts were analyzed by TPR (Figure 6). TPR curves obtained from these samples showed two main reduction steps. The lower temperature peak was attributed to reduction of Fe^{3+} species to Fe_3O_4, and Cr^{6+} to Cr^{3+}. The second peak was due to reduction of Fe_3O_4 to FeO and metallic iron. A high increase of the reduction temperatures for sample prepared by impregnation method was detected. Hydrogen consumption of the first reduction peak for this sample was higher since it was compound of maghemite. Moreover, higher hydrogen consumption was necessary to reduce this sample to FeO and to metallic iron. It seems that presence of initial γ-Fe_2O_3 in the material decreased reducibility of molybdenum-based catalysts and the reduction would not be easy. This behaviour could make very difficult obtaining the active phase for WGS reaction, what could be a serious inconvenient. The replacement of chromium by molybdenum produced a shift of the temperature maximum to higher values. The reduction of Fe^{3+} phases to magnetite were shifted from 300 to 376 ºC and in the case of the high temperature peak from 620 to 750 ºC. This suggests that molybdenum made the formation of metallic iron to be more difficult, increasing the active phase stability. The higher reduction resistance of molybdenum doped material could be related with the lower BET surface area

obtained from this sample, leading to a decrease in the reactivity of the material.

3.3. Effect of Fe/Mo ratio

A series of FeMo catalysts was prepared by oxidation-precipitation method with different Fe/Mo, as mentioned in the experimental section. Lattice parameters obtained from XRD are shown in Table 3. An increase of molybdenum content lead to a contraction of the lattice parameter due to the smaller ionic radius of Mo^{6+} compared to Fe^{2+} and Fe^{3+}. This trend indicates that molybdenum was incorporated into magnetite lattice in all these materials. Average crystallite sizes increased with molybdenum content. Table 1 shows the reduction temperatures of these samples. There were not significant differences between the samples prepared with lower molybdenum contents. The temperature maximum increased for the sample prepared with the lowest Fe/Mo ratio.

As shown in Figure 7, there was a linear relationship between molybdenum content and BET surface area. Specific surface area of samples increased when molybdenum content of catalyst was increased. This fact suggests that molybdenum could act as a structural promoter.

3.4. Addition of copper to Fe-Mo catalysts

FeMo material was promoted with copper to increase the activity of catalyst. X-ray-diffractogram obtained from this sample showed that magnetite was the only crystalline phase and segregated phases of copper or molybdenum were not detected. The lattice parameter of this material (Table 3) was higher than that obtained for AFeMo12 catalyst. When Cu^{2+} replaces Fe, an expansion of the lattice takes place since this cation has an ionic radius (0,87 Å) larger than Fe^{3+} and Fe^{2+}. The lattice parameter of AFeCrCu material was smaller than that for AFeMoCu catalyst since copper was not incorporated into the magnetite lattice in the former.

TEM micrographs obtained from AFeMoCu sample are shown in Figure 8. This material

was composed of spherical particles with sizes between 10 and 50 nm. Addition of copper to FeMo catalysts produced a decrease of crystallite size since substitution of iron by larger metal ions shifted the equilibrium particle size towards smaller particles. These results were in agreement with that obtained by Scherrer equation. Energy dispersive X-ray (EDX) analyses indicated that molybdenum and copper were incorporated into magnetite lattice and the distribution of these metals was homogeneous.

TPR profiles of these samples are shown in Figure 9. The first reduction for AFeMoCu catalyst was shifted to lower temperatures as compared to AFeMo12 and AFeCrCu materials. The second reduction peak appeared at lower temperature than in AFeMo12 catalyst but at higher temperature than AFeCrCu material. Moreover, hydrogen consumption obtained for AFeMoCu sample was the highest one. Therefore, the stability of the magnetite active phase was enhanced in AFeMoCu material; meanwhile the reduction to metallic iron was more difficult.

Molybdenum and copper doped catalyst was tested for WGS reaction (Table 2), obtaining a CO conversion similar to those of AFeCrCu and commercial materials. As well, the product distribution obtained from AFeMoCu sample was analogous to that of the classical catalysts. Hydrogen concentration in the product gas was over 55 % Vol. and CO concentration decreased below 10 % Vol. These results indicate that molybdenum is a promising dopant to replace chromium in high temperature WGS catalysts.

4. Conclusions

The oxidation-precipitation method allows obtaining high temperature WGS catalysts directly in the active phase and their catalytic activity was comparable to that obtained with commercial materials. During the preparation of FeMo catalysts, wet impregnation method produced materials composed by γ-Fe_2O_3 with lower reducibility. This could make their activation to be more difficult. When oxidation-precipitation was used, molybdenum was

totally incorporated into the magnetite lattice for all the range of composition studied. This gave larger crystallite sizes and lower specific surface areas than those of FeCr catalysts, obtaining materials with high thermal stability of the active phase. The properties of molybdenum and copper doped catalysts synthesized by oxidation-precipitation were similar to that of FeCrCu materials in terms of catalytic activity, product distribution and thermal stability.

5. Acknowledgements

The authors acknowledge to the Ministry of Education and Science of Spain, Comunidad de Madrid and Universidad Rey Juan Carlos for funding through projects ENE2004-07758-C02-02, ENE2007-66959 and URJC-CM-2007-CET-1456.

6. References

[1] Ni, M.; Leung, D. Y. C.; Leung, M. K. H.; Sumathy, K. An overview of hydrogen production from biomasa. Fuel Processing Technology 2006; 87: 461-472.

[2] Basagianis, A. C.; Verykios, X. E. Catalytic steam reforming of acetic acid for hydrogen production. International Journal of Hydrogen Energy 2007; 32: 3343-3355.

[3] Wei, L.; Xu, S.; Zhang, L.; Liu, C.; Zhu, H.; Liu, S. Steam gasification of biomass for hydrogen-rich gas in a free-fall reactor. International Journal of Hydrogen Energy 2007; 32: 24-31.

[4] Biswas, P.; Kunzru, D. Steam reforming of ethanol for production of hydrogen over Ni-CeO_2-ZrO_2 catalyst: Effect of support and metal loading". International Journal of Hydrogen Energy 2007; 32: 969-980.

[5] Vizcaíno, A. J.; Carrero, A.; Calles, J. A. Hydrogen production by ethanol steam reforming over Cu-Ni catalysts. International Journal of Hydrogen Energy 2007; 32:

1450-1461.

[6] Sánchez-Sánchez, M. C.; Navarro, R. M.; Fierro, J. L. G. Ethanol steam reforming over Ni/M_xO_y-Al_2O_3 (M = Ce, La, Zr and Mg) catalysts: Influence of support on the hydrogen production. International Journal of Hydrogen Energy 2007; 32: 1462-1471.

[7] Zhang, B.; Tang, X.; Li, Y.; Xu, Y.; Shen, W. Hydrogen production form steam reforming of ethanol and glycerol over ceria supported metal catalysts. International Journal of Hydrogen Energy 2007; 32: 2367-2373.

[8] Ladebeck, J. R.; Wagner, J. P. Catalysis development for water-gas shift. Handbook of fuel Cells-Fundamentals, Technology and Applications 2003; Vol. 3, Part 2: 190-201.

[9] Corella, J.; Aznar, M. P.; Caballero, M. A.; Molina, G.; Toledo, J. M. 140 g H_2/kg biomasa d. a. f. by a CO-shift reactor downstream form a FB biomass gasifier and a catalytic steam reformer. International Journal of Hydrogen Energy 2008; 33:1820-1826.

[10] Rhodes, C.; Hutchings, G. J.; Ward, A. M. Water-gas shift reaction: finding the mechanistic boundary. Catalysis Today 1995; 23: 43-58.

[11] Edwards, M. A.; Whittle, D. M.; Rhodes, C.; Ward, A. M.; Rohan, D.; Shannon, M. D.; Hutchings, G. J.; Kiely, C. J. Microstructural studies of the copper promoted iron oxide/chromia water-gas shift catalyst. Physical Chemistry Chemical Physics 2002; 4: 3902-3908.

[12] Dufour, J; Martos, C.; Ruiz, A.; Carrasco, A. Synthesis of Fe_3O_4-Cr_2O_3 catalysts by oxy-coprecipitation for water gas shift reaction 10th Mediterranean Congress of Chemical Engineering (2005).

[13] Carneiro de Araújo, G.; Rangel, M. C. An environmental friendly dopant for the high-temperature shift catalyst. Catalysis Today 2000; 62: 201-207.

[14] Trimm, D. L. Minimisation of carbon monoxide in a hydrogen stream for fuel cell application. Applied Catalysis A: General 2005; 296 (1): 1-11.

[15] Natesakhawat, S.; Wang, X.; Zhang, L.; Ozkan, U. M. Development of chromium-free iron-based catalysts for high-temperature water-gas shift reaction. Journal of Molecular catalysis A: Chemical 2006; 260: 82-84.

[16] Rangel Costa, J.; Marchetti, G. S.; G.; Rangel, M. C. A thorium-doped catalyst for the high temperature shift reaction. Catalysis Today 2002; 77: 205-213.

[17] Li, K.; Luo, L. T.; Li, F. Y.; Le, Z. P.; Liu, C. H. Journal of Natural Gas Chemistry, 6 (1) (1997), 68-75.

[18] Júnior, I. L.; Millet, J. M. M.; Aouine, M.; Rangel, M. C. The role of vanadium on the properties of iron based catalysts for the water gas shift reaction. Applied Catalysis A: General 2005; 283 (1-2): 91-98.

[19] Khan, A.; Chen, P. Boolchand, P. G. Smirniotis. Modified nano-crystalline ferrites for high-temperature WGS membrane reactor applications". Journal of Catalysis 2008; 253: 91-104.

Figures

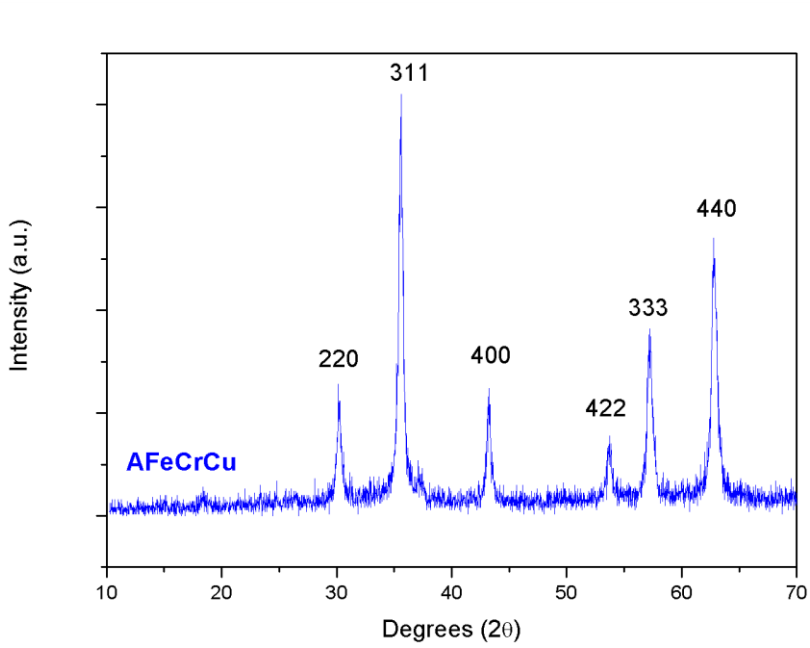

Figure 1. XRD pattern of FeCrCu material prepared by oxidation-precipitation.

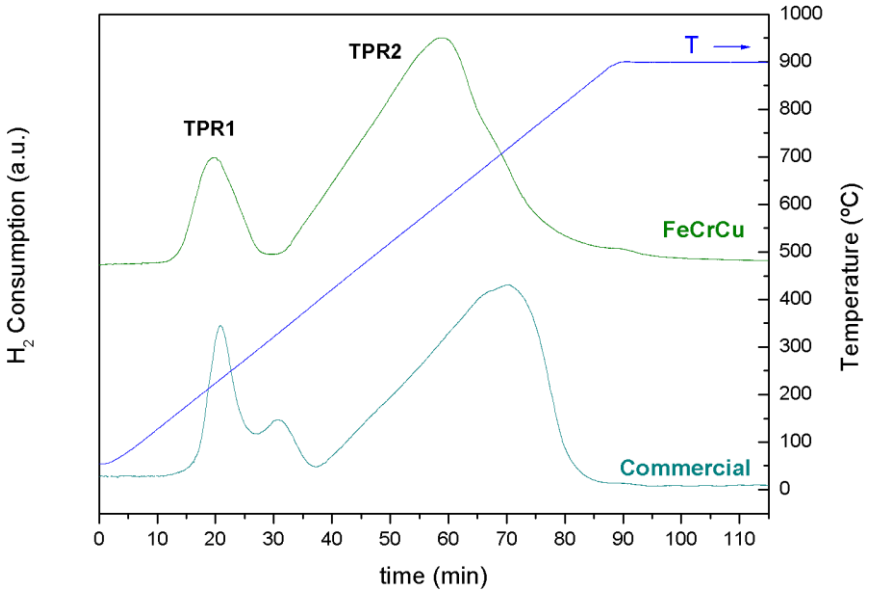

Figure 2. TPR results of commercial catalyst and FeCrCu material prepared by oxidation-precipitation.

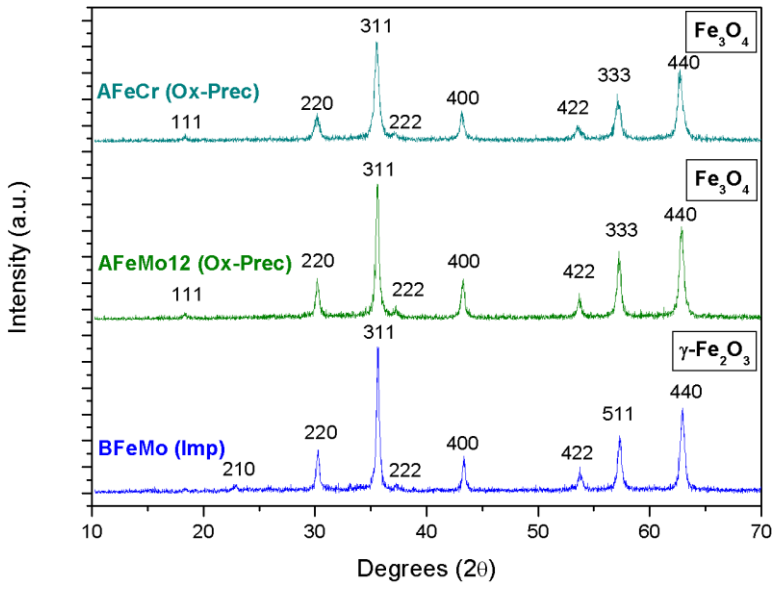

Figure 3. XRD patterns of AFeMo12, BFeMo and AFeCr catalysts.

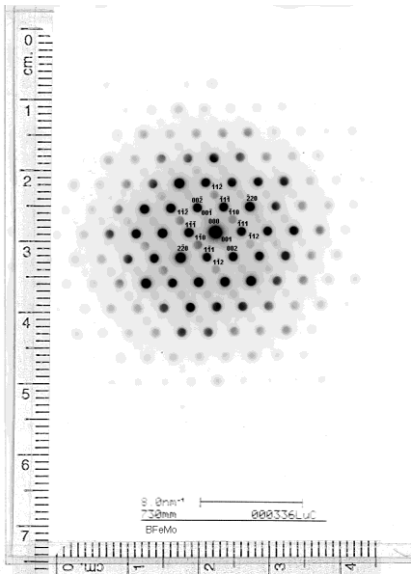

Figure 4. Electron diffraction pattern obtained form BFeMo sample.

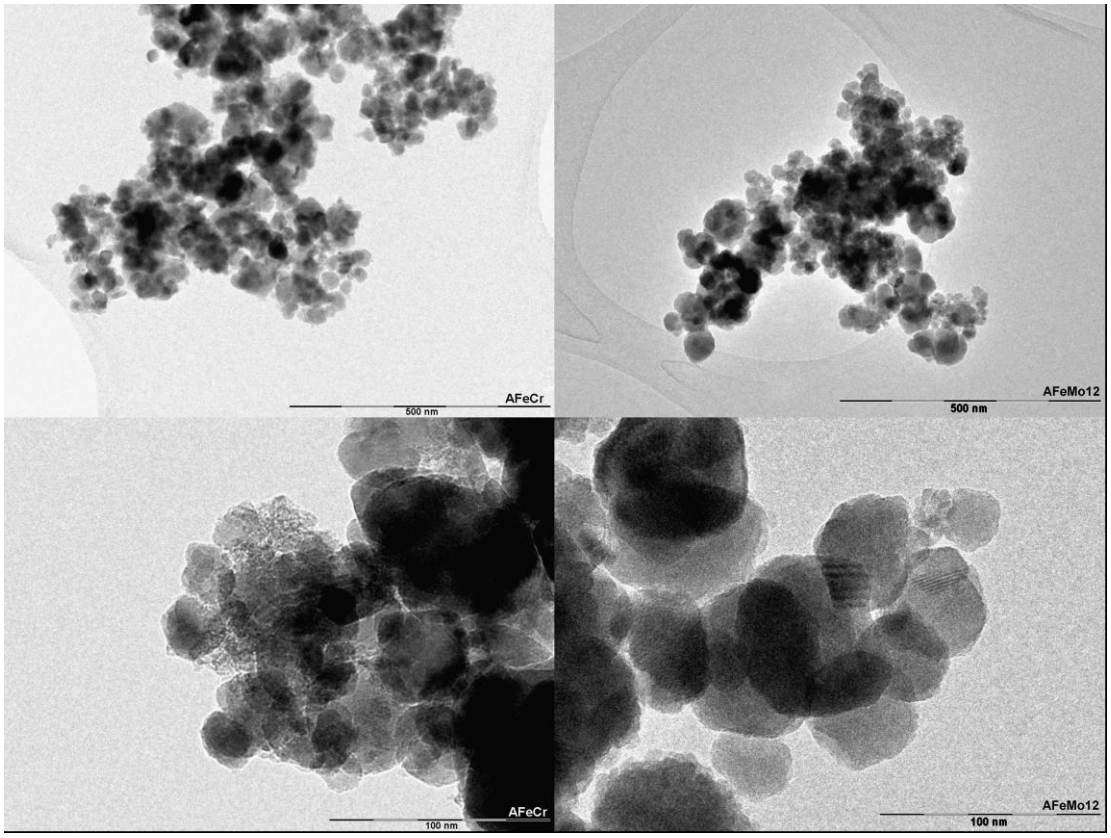

Figure 5. TEM microphotographs of AFeCr and AFeMo12 samples.

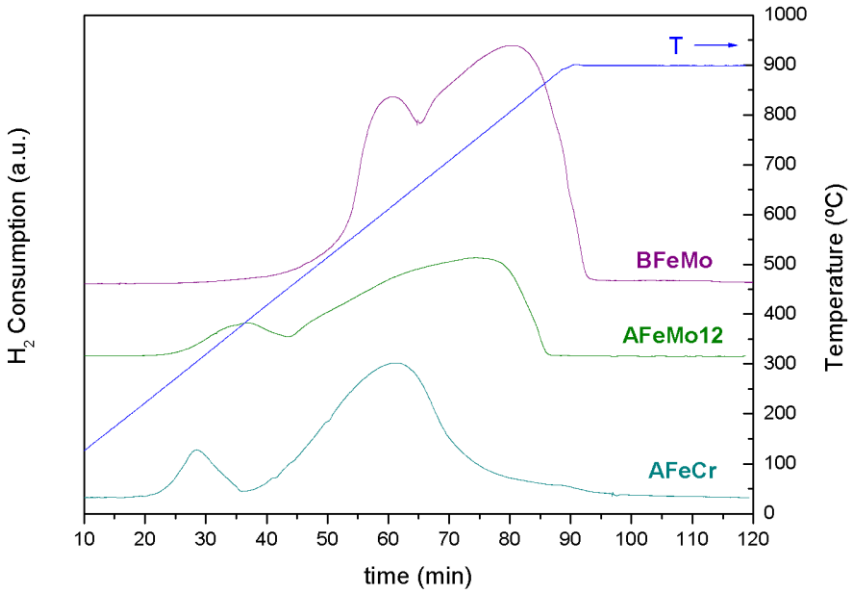

Figure 6. TPR profiles of FeCr and FeMo catalysts prepared by oxidation-precipitation method.

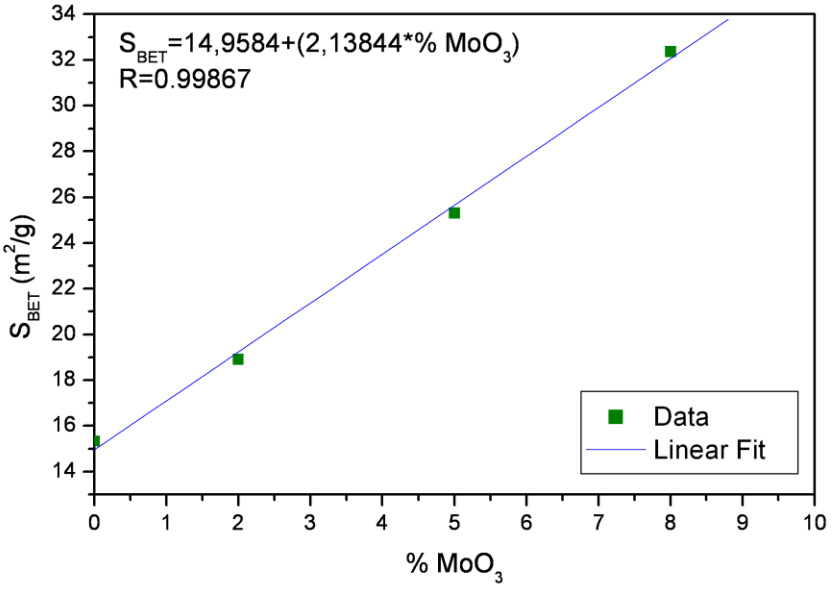

Figure 7. Relationship between specific surface area and molybdenum content to FeMo catalysts.

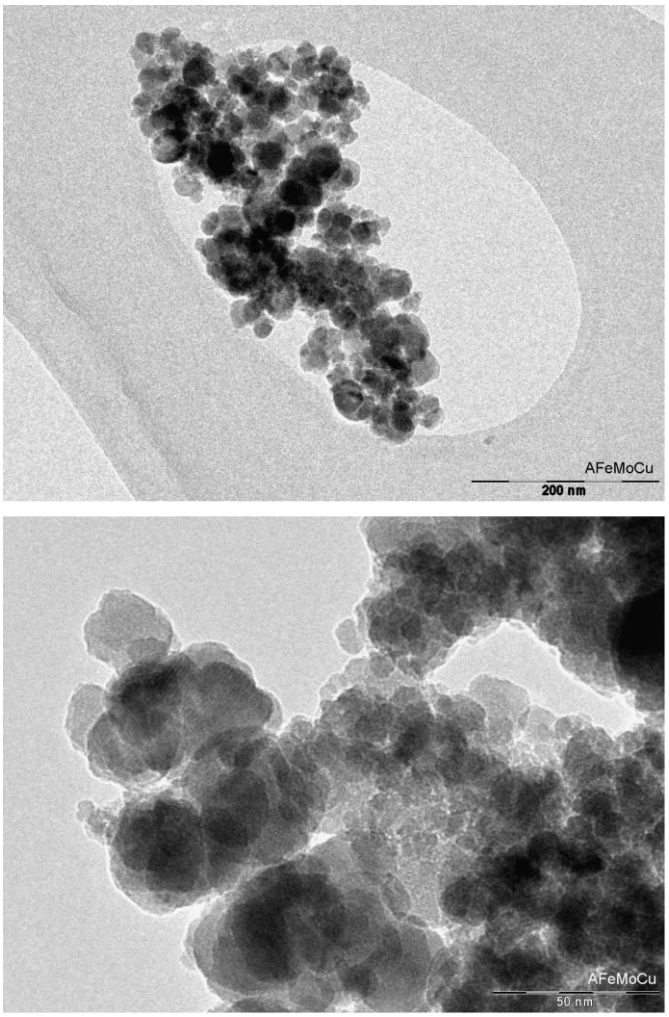

Figure 8. TEM micrographs of FeMoCu sample.

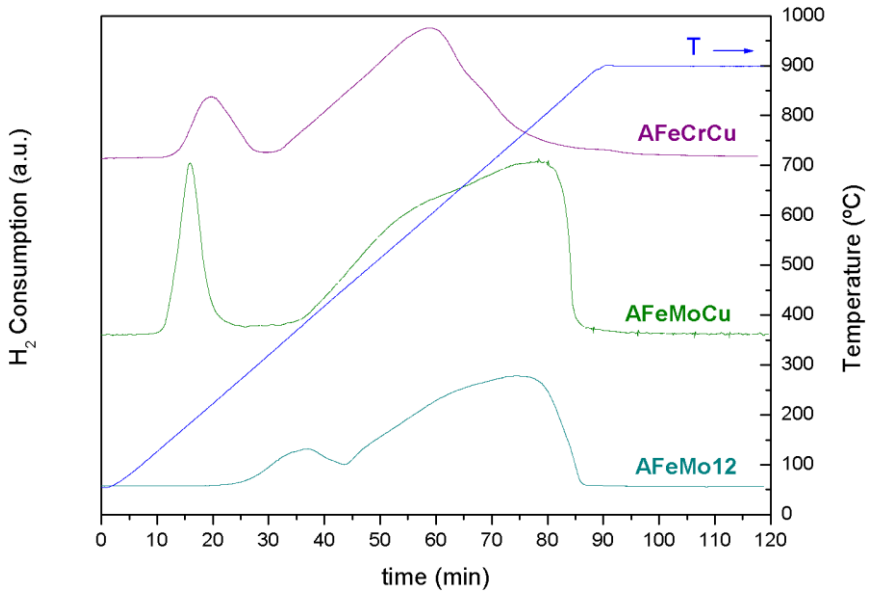

Figure 9. TPR profiles of FeMo, FeMoCu and FeCrCu samples prepared by oxidation-precipitation.

Tables

Table 1. Theoretical Fe/promoter ratios of samples prepared.

Sample	Fe/Cr (wt.)	Fe/Mo (wt.)	Fe/Cu (wt.)
AFeCr	12,2	--	--
AFeCrCu	12,2	--	40,9
AFeMo12	--	12,2	--
AFeMo20	--	20,7	--
AFeMo53	--	53,2	--
AFeMoCu	--	12,2	12,4
BFeMo	--	12,2	--

Table 2. CO conversion and product distribution obtained under WGS reaction.

Sample	X_{CO} (%)	Product Distribution		
		H_2 (% Vol.)	CO_2 (% Vol.)	CO (% Vol.)

Commercial	84	56,2	39,3	6,9
AFeCrCu	79	55,7	38,5	9,1
AFeMoCu	80	57,3	34,2	8,4

Table 3. Characterization results of catalysts prepared.

	XRF			XRD		Ads-Des. N_2	TPR	
Sample[a]	**Fe/Cr (wt.)**	**Fe/Mo (wt.)**	**Fe/Cu (wt.)**	**ao[b] (nm)**	**Dc[c] (nm)**	**S_{BET} (m^2/g)**	**TPR1 (ºC)**	**TPR2 (ºC)**
AFeCr	12,9	--	--	0,8369	15,7	106	303	620
AFeCrCu	12,8	--	39,3	0,8370	18,8	109	220	605
AFeMo12	--	13,4	--	0,8353	26,7	32	376	749
AFeMo20	--	24,2	--	0,8371	22,5	25	341	679
AFeMo53	--	59,9	--	0,8390	20,9	19	340	679
AFeMoCu	--	14,3	16,5	0,8392	18,8	42	181	750
BFeMo	--	13,2	--	0,8357	26,7	12	604	797

[a] A: Samples prepared by oxidation-precipitation method and B: samples prepared by wet impregnation.
[b] ao: Lattice parameter obtained from XRD patterns.
[c] Dc: Crystallite size obtained from XRD results by Scherrer equation.